Structure and stability of quasi-two-dimensional boson-fermion mixtures with vortex-antivortex superposed states

Linghua Wen,[1,2,*] Yongping Zhang,[1,3] and Jian Feng[2]

[1]*Institute of Physics, Chinese Academy of Sciences, Beijing 100190, China*
[2]*Department of Physics, Liaocheng University, Shandong 252059, China*
[3]*Department of Physics and Astronomy, Washington State University, Pullman, Washington, 99164 USA*

(Dated: November 2, 2010)

We investigate the equilibrium properties of a quasi-two-dimensional degenerate boson-fermion mixture (DBFM) with a bosonic vortex-antivortex superposed state (VAVSS) using a quantum-hydrodynamic model. We show that, depending on the choice of parameters, the DBFM with a VAVSS can exhibit rich phase structures. For repulsive boson-fermion (BF) interaction, the Bose-Einstein condensate (BEC) may constitute a petal-shaped "core" inside the honeycomb-like fermionic component, or a ring-shaped joint "shell" around the onion-like fermionic cloud, or multiple segregated "islands" embedded in the disc-shaped Fermi gas. For attractive BF interaction just below the threshold for collapse, an almost complete mixing between the bosonic and fermionic components is formed, where the fermionic component tends to mimic a bosonic VAVSS. The influence of an anharmonic trap on the density distributions of the DBFM with a bosonic VAVSS is discussed. In addition, a stability region for different cases of DBFM (without vortex, with a bosonic vortex, and with a bosonic VAVSS) with specific parameters is given.

PACS numbers: 03.75.Lm, 03.75.Ss

I. INTRODUCTION

With the experimental realizations of atomic Bose-Einstein condensate (BEC), molecular BEC and fermionic condensate, considerable attention has been given to degenerate boson-fermion mixtures (DBFMs) where particles obeying different quantum statistics are intermingled [1, 2]. The DBFMs, such as ^{7}Li-^{6}Li [3, 4], ^{23}Na-^{6}Li [5], ^{87}Rb-^{40}K [6–10], and ^{174}Yb-^{173}Yb [11], have been successfully observed by different experimental groups via interspecies sympathetic cooling. In addition, such mixtures can also be realized from an imbalanced two-component fermi gas where all minority fermions pair up with majority fermions and form a BEC [12, 13].

The collisional interactions between bosons and fermions strongly affect the properties of DBFMs, even though the ultracold mixed gases are very dilute [14–31]. A noticeable example is the structure and stability of a trapped DBFM which has been investigated extensively by several authors. In the case of repulsive boson-fermion (BF) interaction, the system is expected to undergo a mixing-demixing transition with the increase of the repulsion, while in the case of attractive BF interaction the mixture collapses above a critical strength [6, 9, 14–19, 32–35]. In particular, the effect of a bosonic vortex on the stability and the mixing-demixing transition of a DBFM is recently addressed [23, 36]. It is shown that when the BEC sustains a vortex state the DBFM becomes more stable.

In this paper, we consider the equilibrium properties of a quasi-two-dimensional (quasi-2D) DBFM in the presence of a bosonic vortex-antivortex superposed state (VAVSS). Recently, the VAVSS in BECs has attracted extensive research interest as it exhibits peculiar petal-like structure and rich dynamics [37–41]. Furthermore, the VAVSS may have fundamental as well as practical applications in quantum information and inertial sensing. Experimentally, the creation of VAVSS in BECs has been reported by Anderson *et al* [42] and Wright *et al* [43]. Throughout the present work, we use a quantum-hydrodynamic model [36] to investigate the structure of the exact 2D spatial density distributions and the stability of the system against collapse. This mean-field-hydrodynamic model is quite successful in the study of collapse dynamics [16] and dark [44] and bright solitons [24, 45] in a DBFM. The theoretical predictions on fermionic collapse in a DBFM agree well with the experimental results [6, 9], and those on bright solitons are in agreement with a relevant microscopic investigation [46]. We show that, for interspecies repulsion, the bosonic component may form a petal-shaped "core" inside the honeycomb-like fermionic one, or a ring-shaped joint "shell" around the onion-like fermionic cloud, or even segregated "islands" embedded in the disc-shaped Fermi gas. For interspecies attraction below the critical value for collapse, there is an enhanced mixing (even an almost complete mixing) between bosons and fermions, where the fermionic cloud tends to simulate a bosonic VAVSS. Moreover, we find that the DBFM with a bosonic VAVSS and the one with a bosonic pure vortex sustain an intermittent stability diagram.

The paper is organized as follows. In section II we introduce the mean-field-hydrodynamic model for a quasi-2D DBFM, which is comprised of two coupled quantum-hydrodynamic equations. In section III, we present the

*Electronic address: wenlinghua@lcu.edu.cn

numerical results and some discussion on the structure of the exact 2D density profiles of a DBFM with a bosonic VAVSS. Furthermore, a stability region for different cases of DBFM with specific parameters is displayed. The conclusion is outlined in the last section.

II. MEAN-FIELD-HYDRODYNAMIC MODEL FOR A DEGENERATE BOSON-FERMION MIXTURE

We consider a dilute degenerate mixture composed of N_B condensed bosons and N_F spin-polarized fermions at zero temperature, with respective particle mass m_B and m_F. In the case of strong axial (z-direction) confinement, the DBFM reduces to a quasi-2D system, where the axial trap frequency is denoted by ω_z. Here we use the time-dependent mean-field-hydrodynamic model developed in Ref. [36] to describe this BF system. The Lagrangian density of the DBFM reads

$$\mathcal{L} = \mathcal{L}_B + \mathcal{L}_F + \mathcal{L}_{BF}. \tag{1}$$

Here $\mathcal{L}_B$ is the ordinary bosonic Lagrangian density,

$$\begin{aligned}\mathcal{L}_B &= \frac{i\hbar}{2}(\Psi_B^*\frac{\partial\Psi_B}{\partial t} - \Psi_B\frac{\partial\Psi_B^*}{\partial t}) - \frac{\hbar^2}{2m_B}(\left|\frac{\partial\Psi_B}{\partial x}\right|^2 \\ &+ \left|\frac{\partial\Psi_B}{\partial y}\right|^2) - V_B n_B - \frac{g_{BB}}{2}n_B^2,\end{aligned} \tag{2}$$

where $\Psi_B(x,y,t)$ is the hydrodynamic field of the Bose gas, i.e., the macroscopic BEC wave function, $n_B = |\Psi_B|^2$ is the 2D bosonic density with normalization $N_B = \iint |\Psi_B|^2\, dxdy$, and V_B is the external trapping potential for the bosons. $g_{BB} = 2\sqrt{2\pi}\hbar^2 a_{BB}/(a_{zB}m_B)$ is the 2D interatomic interaction strength with a_{BB} being the 3D boson-boson (BB) s-wave scattering length and $a_{zB} = \sqrt{\hbar/(m_B\omega_z)}$ the axial harmonic length of bosons. The bosonic Lagrangian density $\mathcal{L}_B$ can describe well all the dynamical properties of the dilute quasi-2D BEC (see Ref. [36] and references therein). For simplicity, here we have assumed the BEC to be strictly 2D.

The Lagrangian density of the Fermi gas $\mathcal{L}_F$ is expressed by [36]

$$\begin{aligned}\mathcal{L}_F &= \frac{i\hbar}{2}(\Psi_F^*\frac{\partial\Psi_F}{\partial t} - \Psi_F\frac{\partial\Psi_F^*}{\partial t}) - \frac{\hbar^2}{6m_F}(\left|\frac{\partial\Psi_F}{\partial x}\right|^2 \\ &+ \left|\frac{\partial\Psi_F}{\partial y}\right|^2) - V_F n_F - \xi_F(n_F),\end{aligned} \tag{3}$$

where $\Psi_F(x,y,t)$ is the hydrodynamic field of the degenerate Fermi gas (DFG) (i.e., an average fermionic wave function), $n_F = |\Psi_F|^2$ is the 2D fermionic density with normalization $N_F = \iint |\Psi_F|^2\, dxdy$, and V_F is the external trapping potential for the fermions. $\xi_F(n_F)$ denotes the zero-temperature bulk energy density of an ideal quasi-2D Fermi gas under axial harmonic confinement, and it reads

$$\xi_F = \begin{cases} \hbar\omega_z\pi(n_F a_{zF})^2, & 0 \leqslant n_F a_{zF}^2 < \frac{1}{2\pi}, \\ \frac{\hbar\omega_z}{6\pi a_{zF}^2}(4\pi n_F a_{zF}^2 - 1)^{3/2} + \frac{1}{12\pi}, & n_F a_{zF}^2 \geqslant \frac{1}{2\pi}. \end{cases} \tag{4}$$

For $0 \leqslant n_F < 1/(2\pi a_{zF}^2)$, the Fermi gas is strictly 2D, where $a_{zF} = \sqrt{\hbar/(m_F\omega_z)}$ is the axial harmonic length of fermions. For $n_F \geqslant 1/(2\pi a_{zF}^2)$, the Fermi gas has the 2D-3D crossover, where several single-particle modes of the harmonic oscillator along the z axis are occupied. The Fermi gas becomes 3D for $n_F \gg 1/(2\pi a_{zF}^2)$. Due to the Pauli exclusion principle, the interaction between identical fermions in spin polarized state is highly suppressed and has been neglected in the Lagrangian density $\mathcal{L}_F$ and will be neglected throughout this paper. The second term $-\hbar^2|\nabla_{x,y}\Psi_F|^2/6m_F$ in Eq.(3) represents the Thomas-Fermi-Weizsäcker kinetic energy which includes the surface kinetic energy due to spatial variation [19]. Note that the fermionic Lagrangian density $\mathcal{L}_F$ can only be safely used to describe the static and collective properties of the quasi-2D Fermi gas [36]. As the strict 2D Fermi gas requiring a very small number of particles is not the case of real experiments, we take into account the 2D-3D crossover in the fermionic component.

It may not be entirely proper to define an average fermionic wave function Ψ_F for a DFG. A proper treatment of the DFG should be performed using a fully antisymmetrized many-body Slater determinant wave function. However, the probability density n_F of a DFG calculated in this way should lead to reasonable results [14] and has led to proper probability distribution for a DFG [16, 19] as well as results for collapse of a DFG [16, 19, 32] in agreement with experiment. This method has also been used successfully to predict fermionic bright and dark solitons in a DBFM [24, 44]. The virtue of the mean-field-hydrodynamic model for a DFG over a microscopic description is its simplicity and good predictive power. Similar mean-field treatment for degenerate fermions can also be found in Refs. [47, 48].

Finally, the Lagrangian density $\mathcal{L}_{BF}$ for BF interaction is given by

$$\mathcal{L}_{BF} = -g_{BF}n_B n_F, \tag{5}$$

where $g_{BF} = 2\pi a_{BF}\hbar^2/(m_{BF}\sqrt{2\pi a_{zB}a_{zF}})$ is the coupling constant of BF interaction in terms of the 3D BF s-wave scattering length a_{BF} and the BF reduced mass $m_{BF} = m_B m_F/(m_B + m_F)$.

In terms of Eqs. (1)-(5), the Euler-Lagrange equations of motion become

$$\begin{aligned}i\hbar\frac{\partial}{\partial t}\Psi_B &= [-\frac{\hbar^2}{2m_B}(\frac{\partial^2}{\partial x^2} + \frac{\partial^2}{\partial y^2}) + V_B + g_{BB}|\Psi_B|^2 \\ &+ g_{BF}|\Psi_F|^2]\Psi_B,\end{aligned} \tag{6}$$

$$\begin{aligned}i\hbar\frac{\partial}{\partial t}\Psi_F &= [-\frac{\hbar^2}{6m_F}(\frac{\partial^2}{\partial x^2} + \frac{\partial^2}{\partial y^2}) + V_F + \mu_F \\ &+ g_{BF}|\Psi_B|^2]\Psi_F.\end{aligned} \tag{7}$$

Here $\mu_F = \partial\xi_F/\partial n_F$ is the bulk chemical potential of the non-interacting Fermi gas in the 2D-3D crossover, which is expressed by

$$\mu_F = \begin{cases} 2\pi\hbar\omega_z n_F a_{zF}^2, & 0 \leqslant n_F a_{zF}^2 < \frac{1}{2\pi}, \\ \hbar\omega_z\sqrt{4\pi n_F a_{zF}^2 - 1}, & n_F a_{zF}^2 \geqslant \frac{1}{2\pi}. \end{cases} \tag{8}$$

The resultant quantum-hydrodynamic equations have a nonpolynomial nonlinearity for the fermionic component as shown in Eqs. (6), (7) and (8).

For simplicity, we assume that the 2D radial trapping potentials for the bosonic and fermionic components are the same and take the forms

$$V_B(x,y) = V_F(x,y) = \frac{1}{2}m_B\omega_\perp^2\left[x^2+y^2+\lambda\frac{(x^2+y^2)^2}{a_0^2}\right], \tag{9}$$

where $a_0 = \sqrt{\hbar/(m_B\omega_\perp)}$ is the radial harmonic length of bosons with $\omega_\perp$ the radial trap frequency as seen by the bosons. The quartic term in Eq.(9) denotes the anharmonicity of the traps, which is possibly caused by experimental uncertainties or artificial quartic confinement. λ is a dimensionless parameter that determines the relative strength of the quartic component for bosons. Our choice of the trapping potentials corresponds to a reduction of $\omega_\perp$ by a factor $\sqrt{m_B/m_F}$ as in the study by Modugno *et al* [32] and a reduction of λ by a factor $\sqrt{m_B/m_F}$, where the two assumptions give a simpler analytical form of the final dynamic equations without any consequence to our qualitative study. Recent studies show that the quartic distortion influences the rotational properties [49] and the collective excitations [50] of BECs. An interesting question is whether the additional quartic distortion influences the structure and stability of a DBFM.

Eqs. (6) and (7) can be renormalized to dimensionless form. By introducing the notations $x_0 = x/a_0$, $y_0 = y/a_0$, $\eta = t\omega_\perp$, $\rho = m_B/m_F$, $c = g_{BB}N_B/(\hbar\omega_\perp a_0^2)$, $f = g_{BF}N_F/(\hbar\omega_\perp a_0^2)$, $k = g_{BF}N_B/(\hbar\omega_\perp a_0^2)$, $\psi_B = a_0\Psi_B/\sqrt{N_B}$ and $\psi_F = a_0\Psi_F/\sqrt{N_F}$, we obtained the rescaled Euler-Lagrange equations for the mixture

$$\begin{aligned} i\frac{\partial}{\partial\eta}\psi_B &= [-\frac{1}{2}(\frac{\partial^2}{\partial x_0^2}+\frac{\partial^2}{\partial y_0^2})+\frac{1}{2}(x_0^2+y_0^2)+\frac{\lambda}{2}(x_0^2+y_0^2)^2 \\ &\quad +c\left|\psi_B\right|^2+f\left|\psi_F\right|^2]\psi_B, \end{aligned} \tag{10}$$

$$\begin{aligned} i\frac{\partial}{\partial\eta}\psi_F &= [-\frac{\rho}{6}(\frac{\partial^2}{\partial x_0^2}+\frac{\partial^2}{\partial y_0^2})+\frac{1}{2}(x_0^2+y_0^2)+\frac{\lambda}{2}(x_0^2+y_0^2)^2 \\ &\quad +\mu_{0F}+k\left|\psi_B\right|^2]\psi_F, \end{aligned} \tag{11}$$

where $n_{j0} = \left|\psi_j\right|^2 (j = B, F)$ are the rescaled bosonic and fermionic densities. Here the rescaled bulk chemical potential of the Fermi gas with $\gamma = \omega_z/\omega_\perp$ reads

$$\mu_{0F} = \begin{cases} 2\pi\rho N_F\left|\psi_F\right|^2, & 0 \leqslant (\frac{1}{\gamma})\rho N_F\left|\psi_F\right|^2 < \frac{1}{2\pi}, \\ \sqrt{4\pi\rho\gamma N_F\left|\psi_F\right|^2-\gamma^2}, & (\frac{1}{\gamma})\rho N_F\left|\psi_F\right|^2 \geqslant \frac{1}{2\pi}. \end{cases} \tag{12}$$

For the case of a DBFM sustaining a bosonic vortex, a mixing-demixing transition and a collapse in the mixture have been predicted by Adhikari *et al* [36]. In view of the recent studies of VAVSS in BECs [37–43] it is of interest to see how the structure and the stability of a DBFM modify when the Bose gas is in a VAVSS. The appearance of a quantized VAVSS as well as a pure vortex state is the genuine confirmation of phase coherence and superfluidity of the boson component in the DBFM. As the VAVSS can stably exist in nonrotated BECs [37, 38], we consider the bosonic VAVSS of the dimensionless form [41]

$$\psi_B = Ae^{-(x_0^2+y_0^2)/2\sigma^2}e^{i\delta}[\alpha(x_0+iy_0)^l+\beta e^{i\phi}(x_0-iy_0)^l], \tag{13}$$

where A is the normalization constant, σ denotes the width of BEC, δ is a constant phase which may be taken to be zero without loss of generality, and l is the winding number describing the quantum circulation. The real parameters α, β characterize the proportion of the vortex and antivortex with $\alpha^2+\beta^2 = 1$. The relative phase ϕ between the vortex and the antivortex just causes offset of the density distribution by an angle $\phi/2l$.

III. RESULTS AND DISCUSSION

Here we numerically solve the coupled quantum-hydrodynamic equations (10) and (11) with bulk chemical potential μ_{0F} given by Eq. (12) and a trial bosonic VAVSS with definite ratio of α^2 and β^2. The trial solution of the fermionic component is chosen as a Gaussian wave function. In view of the petal-like structure of the VAVSS in BECs, we perform exact 2D numerical calculations which require an enormous computation effort. In our numerical simulation, we consider the ^{87}Rb-^{40}K mixture with m_B being the mass of ^{87}Rb atom and m_F the mass of ^{40}K atom, and take $\omega_z/2\pi = 100$ Hz, $\gamma = 10$. In order to investigate the structure and stability of the DBFM with a bosonic VAVSS, we seek the stationary solution of Eqs. (10) and (11) in the presence of a bosonic VAVSS (13). There are several typical numerical approaches for obtaining the stationary solution of a nonlinear Schödinger equation, for instance, the Newton relaxation method [51] and the imaginary time propagation (ITP) method [38, 52]. In this paper, we obtain the ground state of the DBFM with a bosonic VAVSS by using the ITP method based on the split-step Fourier algorithm [53]. Our preliminary study shows that the petal structure of a VAVSS with $\alpha^2 \neq \beta^2$ only emerges under the condition of extremely weak interatomic interaction or very small particle number, which is usually not met in experiments. For a VAVSS with $\alpha^2 = \beta^2 = 1/2$, however, the petal structure always appears for arbitrary value of the interatomic interaction or the particle number. So we shall mainly consider the case of $\alpha^2 = \beta^2 = 1/2$. The relative phase is taken to be $\phi = 0$ throughout this paper. The BB and BF interactions can be arbitrarily tuned by the Feshbach resonance technique through varying a background magnetic field [2].

Firstly, we consider the solutions of system in the absence of interspecies interaction. In figure 1 we show the 2D bosonic density distribution $n_{B0}(x_0, y_0)$ (top), the 2D fermionic one $n_{F0}(x_0, y_0)$ (middle), and the column density distributions $n_{j0}(x_0, y_0 = 0)$ $(j = B, F)$ of the bosonic and fermionic components (bottom) in a DBFM with a bosonic VAVSS, where $N_B = 1000$, $N_F = 100$, $l = 1$, $\alpha^2 = \beta^2 = 1/2$, $a_{BB} = 40$ nm, $a_{BF} = 0$, and the anharmonic parameters are $\lambda = 0$ (left) and $\lambda = 0.1$ (right), respectively. The bosonic component in the mixture exhibits a petal-like structure (see figures 1(a) and (d)), which is similar to the case of a pure BEC. At the same time the fermionic component displays a Gaussian distribution due to the absence of BF interaction, as shown in figures 1(b) and (e). Comparing with the case of a harmonic potential ($\lambda = 0$, see figures 1(a) and (b)), the density distributions $n_{B0}(x_0, y_0)$ and $n_{F0}(x_0, y_0)$ in the presence of an anharmonic term ($\lambda = 0.1$, see figures 1(d) and (e)), i.e., in the presence of a quartic distortion, become more tightly confined. This can also be seen in the column density distributions $n_{j0}(x_0, y_0 = 0)$ $(j = B, F)$ along the x_0 axis (figures 1(c) and (f)). Thus the additional quartic distortion may favor the sympathetic cooling between the bosons and the fermions, and makes the mixture more stable. Our numerical simulation shows that when $\lambda \neq 0, 0.1$ the density distributions $n_{B0}(x_0, y_0)$ and $n_{F0}(x_0, y_0)$ are similar to those in the case of $\lambda = 0$, i.e., the basic structure of the DBFM is not affected by the quartic distortion. The conclusion is the same in the presence of BF interaction. So in the following we illustrate the equilibrium properties of the DBFM with a bosonic VAVSS with $\lambda = 0$.

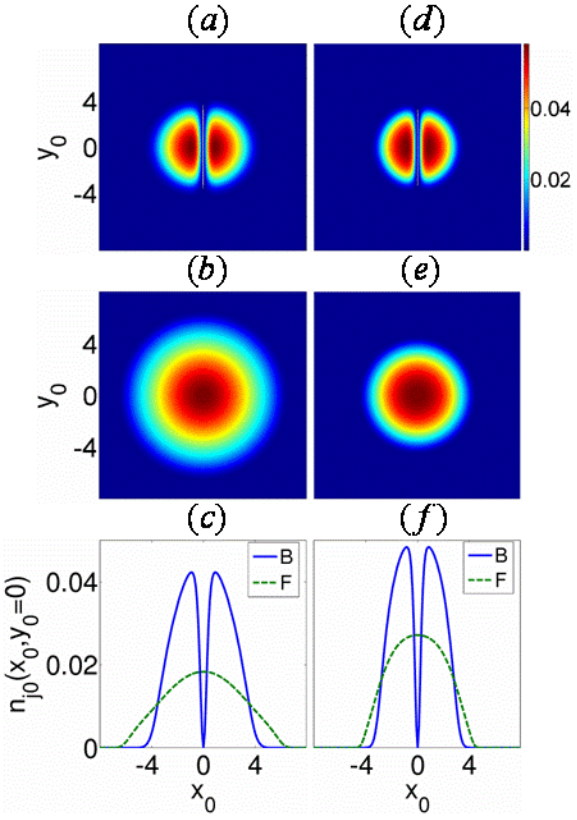

FIG. 1: (color online) Bosonic density distribution $n_{B0}(x_0, y_0)$ (top), fermionic density distribution $n_{F0}(x_0, y_0)$ (middle), and column density distributions $n_{j0}(x_0, y_0 = 0)$ $(j = B, F)$ (bottom) for a DBFM with a bosonic VAVSS in the absence of BF interaction. The anharmonic parameters are $\lambda = 0$ (left) and $\lambda = 0.1$ (right), respectively. Here $N_B = 1000$, $N_F = 100$, $l = 1$, $\alpha^2 = \beta^2 = 1/2$, and $a_{BB} = 40$ nm.

When the BF interaction is nonzero, the DBFM with a bosonic VAVSS can display rich phase structures. Figure 2 gives the density distribution $n_{F0}(x_0, y_0)$ of fermions (left) and the column density distributions $n_{j0}(x_0, y_0 = 0)$ $(j = B, F)$ of bosons and fermions (right) for various BF interactions, where $\lambda = 0$, $N_B = 1000$, $N_F = 100$, $l = 1$, $\alpha^2 = \beta^2 = 1/2$, $a_{BB} = 40$ nm. As shown in figures 2(a) and (d), for repulsive $a_{BF} = 90$ nm the system is in a partial mixed state, where the bosonic component with a petal-like structure lies inside the fermionic one while the fermionic cloud shows a honeycomb-like structure due to the BF repulsion. For a sufficiently large repulsive $a_{BF} = 190$ nm, the fermionic cloud is completely expelled outside the BEC (see figures 2(b) and (e)), which is usually referred as demixing, i.e., the system is in a complete phase-separated state. The phenomenon of mixing-demixing transition has also been found in previous theoretical studies of a DBFM [14, 19, 34] or a DBFM with a bosonic vortex [36]. For the DBFM with a bosonic VAVSS, however, with the increase of BF repulsion the DFG can not be completely expelled from the central region of the harmonic trap due to the bosonic VAVSS. In the case of attractive BF interaction ($a_{BF} < 0$) we find that the fermionic component is pulled inside the bosonic one and the maximum mixing between the two components is then achieved for a critical value of a_{BF}. With the further increase of the strength of the attractive BF interaction the system collapses. In figures 2(c) and (f), where $a_{BF} = -90$ nm, just below the threshold for collapse, we can see an almost complete mixing between the bosonic and fermionic clouds. In this mixed state, the fermionic density distribution developes a petal-like structure reminiscent of a VAVSS as in the bosonic component. However, near the center of the trap the fermionic density $n_{F0}(x_0 = 0, y_0)$ tends to a nonzero constant value and does not have the VAVSS behavior. For a VAVSS with $l = 1$ and $\alpha^2 = \beta^2 = 1/2$, the probability density in the gap regions between two petals should be zero. Therefore the fermionic component is not really in a VAVSS but tends to mimic a bosonic VAVSS due to mixing.

Depending on the choice of parameters the separated phase may exhibit different configurations. Shown in figure 3 are the bosonic density distribution $n_{B0}(x_0, y_0)$ (top), the fermionic one $n_{F0}(x_0, y_0)$ (middle), and the column density distributions $n_{j0}(x_0, y_0 = 0)$ $(j = B, F)$ (bottom) in a DBFM with a bosonic VAVSS for the case of equal particle numbers $N_B = N_F = 1000$. Here $\lambda = 0$,

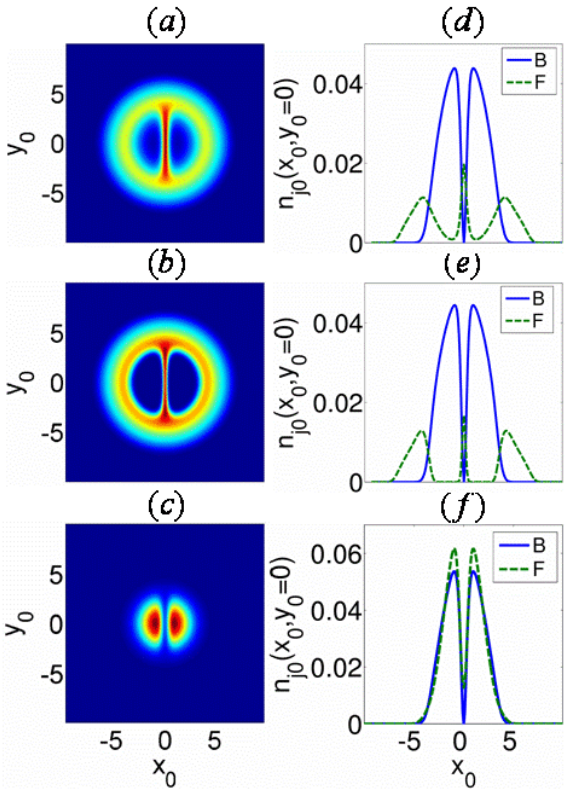

FIG. 2: (color online) Fermionic density distribution $n_{F0}(x_0, y_0)$ (left) and column density distributions $n_{j0}(x_0, y_0 = 0)$ $(j = B, F)$ (right) of a DBFM in the presence of a bosonic VAVSS, where $\lambda = 0$, $N_B = 1000$, $N_F = 100$, $l = 1$, $\alpha^2 = \beta^2 = 1/2$, and $a_{BB} = 40$ nm. The BF scattering lengths are $a_{BF} = 90$ nm (top), $a_{BF} = 190$ nm (middle), and $a_{BF} = -90$ nm (bottom), respectively.

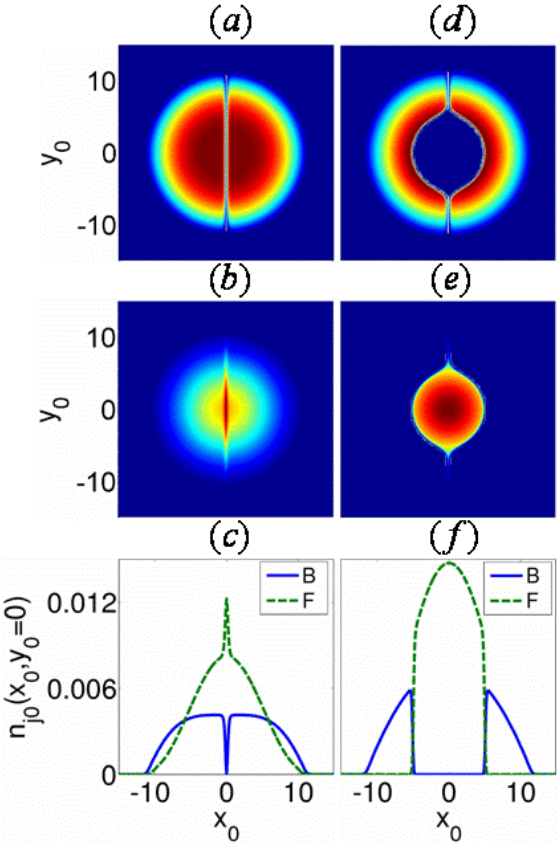

FIG. 3: (color online) Bosonic density distribution $n_{B0}(x_0, y_0)$ (top), fermionic density distribution $n_{F0}(x_0, y_0)$ (middle), and column density distributions $n_{j0}(x_0, y_0 = 0)$ $(j = B, F)$ (bottom) for a DBFM with a bosonic VAVSS in the case of $N_B = N_F = 1000$. The BF s-wave scattering lengths are $a_{BF} = 500$ nm (left) and $a_{BF} = 2000$ nm (right), respectively. The other parameters are $l = 1$, $\alpha^2 = \beta^2 = 1/2$, and $a_{BB} = 2000$ nm.

$l = 1$, $\alpha^2 = \beta^2 = 1/2$, $a_{BB} = 2000$ nm, and the BF s-wave scattering lengths are $a_{BF} = 500$ nm (left) and $a_{BF} = 2000$ nm (right), respectively. It is easy to confirm that the diluteness condition of the gases is satisfied for all the parameters mentioned in this paper. From figures 3(a)-(c), we can see for $a_{BF} = 500$ nm and given parameters the system is in a perfect mixed state, where the fermionic density reaches the maximum in the gap region between two bosonic petals because of the BF repulsion. For sufficiently strong BF repulsion $a_{BF} = 2000$ nm, the bosons are completely expelled from the center of the trap as shown in figure 3(d), forming a ring-shaped joint "shell" around the fermions due to the presence of the VAVSS. At the same time the fermionic component develops an onion-like core, which can be seen in figure 3(e). The column density distributions $n_{j0}(x_0, y_0 = 0)$ $(j = B, F)$ are illustrated in figure 3(f). Figures 3(d)-(f) definitely indicate a new separated phase of the DBFM which is different from that in figures 2(b) and (e), where though the fermions are completely expelled outside the bosons there is remarkable fermionic density along the axis of $x_0 = 0$ in the trap center.

In figure 4, we display the bosonic and fermionic density distributions $n_{j0}(x_0, y_0)$ $(j = B, F)$ as well as the column density distributions $n_{j0}(x_0, y_0 = 0)$ $(j = B, F)$ for the case of $N_B = 100$ and $N_F = 1000$, where the interspecies s-wave scattering lengths are $a_{BF} = 800$ nm (left) and $a_{BF} = 8000$ nm (right), respectively. The other parameters are $\lambda = 0$, $l = 1$, $\alpha^2 = \beta^2 = 1/2$, and $a_{BB} = 800$ nm. For repulsive $a_{BF} = 800$ nm the DBFM begins to evolve into a coexistence phase of component mixing and separation, where the bosonic component forms two distant and segregated "islands" embedded in the disc-shaped fermionic gas (see figures 4(a)-(c)). When $a_{BF} = 8000$ nm the two bosonic "islands" become more compact and closer, and the fermionic component is completely separated from the bosonic one (see figures 4(d)-(f)). As shown in figure 4(f), the fermionic component constitutes both a "shell" around and a "core" inside the BEC along the x_0-direction, i.e., the Fermi gas distributes on both sides of the Bose gas along the x_0-direction, which is similar to that found in Ref. [14]. However, the layer distribution of the present separated

phase is only along the x_0-direction in the nearby region of $y_0 = 0$ and is absent along the y_0-direction, i.e., the present separated phase does not show 2D or 3D layer configuration. Furthermore, the core structure or the core plus shell structure of the fermionic cloud in a DBFM without vortex can be achieved by varying the BF interaction continuously [14], whereas the different separated phases in the DBFM with a bosonic VAVSS correspond respectively the different parameter conditions and can not be achieved by merely change the BF coupling continuously. The above analysis indicates that the inlay configuration of the two bosonic "islands" embedded in the disc-shaped Fermi gas is a novel separated phase. We expect that this novel separated phase can be observed and tested in the future experiments. For large a_{BF} the fermions could possibly form p-wave pairing, which is beyond the scope of the mean-field treatment. The two compact bosonic segregated "islands" in figure 4(d) perhaps can be understood as a consequence of buoyancy in the Fermi sea.

The BF interaction has a very strong influence not only on the structure of the DBFM with a bosonic VAVSS but also on the stability of the system. For a repulsive BF interaction (positive a_{BF}), a stable structure can always be achieved for a fixed N_B, N_F, λ, l, α, β, ϕ, and BB scattering length a_{BB} as shown in figures 2-4. However, for a sufficiently strong attractive BF interaction (negative a_{BF}), the system can undergo a simultaneous collapse of the bosonic and fermionic density distributions. Physically, the critical value of BF scattering length is determined by the balance between the repulsion of bosons and fermions and the mutual attractive BF interaction. Likewise, when the boson number N_B or fermion number N_F are sufficiently large, the attractive BF interaction can not be stabilized by the repulsions in BB and BF subsystems. Thus the mixture lowers its energy via increasing the boson and fermion densities, and finally the bosonic component or the fermionic one or both the bosonic and fermionic components collapse simultaneously due to instability. In our investigation, the instability signature is found by monitoring the failure of the numerical iterative process, i.e., the invalidation of the coupled equations (10) and (11) describing the DBFM with conserved quantities N_B and N_F. In fact, an indefinite growth of the maximum of the bosonic and fermionic densities always indicates the appearance of an instability onset, and therefore the collapse of the mixture is triggered and unavoidable. This approach is accurate and reliable [23].

The stability region in the plane spanned by $\log(N_F)$ and $\log(N_B)$ is shown in figure 5. As an illustration, we assume the BB and BF scattering lengths of the ^{87}Rb-^{40}K mixture are $a_{BB} = 5$ nm and $a_{BF} = -15$ nm which are very close to the typical experimental values $a_{BB} = 5.25$ nm and $a_{BF} = -13.8$ nm reported by Ferrari *et al* [54]. The four different curves (square, circle, triangle, and inverted triangle) in the figure 5 mark the stability limit for four different cases of DBFM: (i) DBFM without vortex, (ii) DBFM with a bosonic VAVSS of $l = 1$ and $\alpha^2 = \beta^2 = 1/2$, (iii) DBFM with a bosonic VAVSS of $l = 1$, $\alpha^2 = 3/4$ and $\beta^2 = 1/4$, and (iv) DBFM with a bosonic vortex of $l = 1$, respectively. The region below each curve denotes the stability region of the mixture, and that above each curve corresponds to the instability (collapse) one of the system. The stability curves in the range of $\log(N_F) \leqslant 2$ are four almost overlapped and parallel horizontal lines (data not shown here) which are similar to those in the range of $\log(N_F) \geqslant 3.9$.

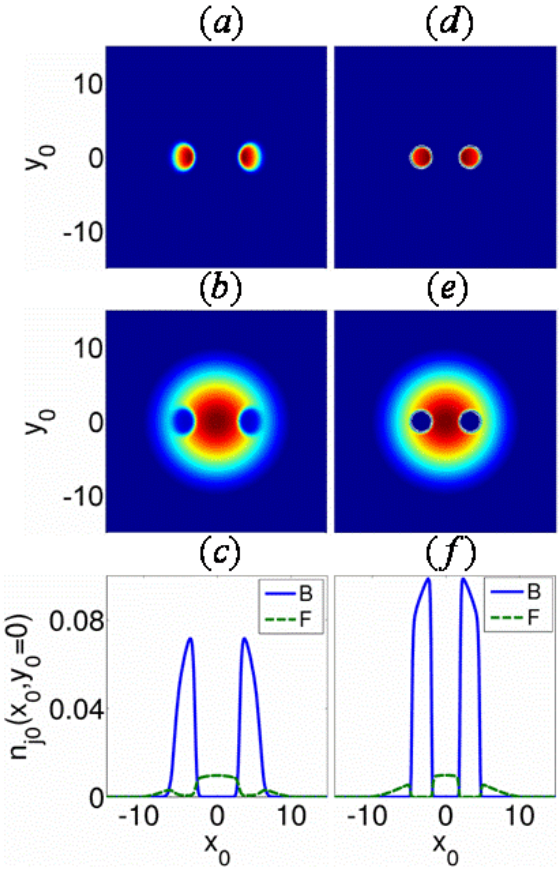

FIG. 4: (color online) Bosonic density distribution $n_{B0}(x_0, y_0)$ (top), fermionic density distribution $n_{F0}(x_0, y_0)$ (middle), and column density distributions $n_{j0}(x_0, y_0 = 0)$ $(j = B, F)$ (bottom) for a DBFM with a bosonic VAVSS in the case of $N_B = 100$ and $N_F = 1000$. The BF s-wave scattering lengths are $a_{BF} = 800$ nm (left) and $a_{BF} = 8000$ nm (right), respectively. The other parameters are $l = 1$, $\alpha^2 = \beta^2 = 1/2$, and $a_{BB} = 800$ nm.

From figure 5 we can see for the same parameters the DBFM with a bosonic vortex is more stable than the one without vortex due to the repulsive centrifugal kinetic energy, in agreement with previous study [36]. In addition, for the case of $N_F \leqslant \text{int}(10^{3.8}) \approx 6310$ the DBFM with a bosonic vortex is more stable than that with a bosonic VAVSS because the energy of a VAVSS (especially, a VAVSS with equal proportions $|\alpha| = |\beta|$) is higher than that of a pure vortex (or antivortex) for a given l [38].

However, for the case of $6310 < N_F < \mathrm{int}(10^{3.9}) \approx 7943$ we find that the DBFM with a bosonic VAVSS is more stable than that with a bosonic vortex. Notice that for attractive BF interaction the fermionic density distribution tends to simulate the bosonic one (see figure 2(c)), thus the overlap region between the bosons and fermions in a DBFM with a bosonic VAVSS is smaller than that in a DBFM with a bosonic vortex due to the petal-like structure of VAVSS. This effect dominates the stability of the system when the number of fermions is sufficiently large such that the influence of the BF attraction on the collapse of a DBFM with a bosonic VAVSS is weaker than that of a DBFM with a bosonic vortex, which is a probable reason for the above intermittency phenomenon in the stability region. At the same time, there is also an intermittency phenomenon between the stability curve for the DBFM with a bosonic VAVSS of $\alpha^2 = 1/2$ and that of $\alpha^2 \neq 1/2$ (e.g., $\alpha^2 = 3/4$). The analysis is similar to the above discussion. Note that the stability curve for the DBFM with a bosonic VAVSS of $l = 1$, $\alpha^2 = 1/4$ and $\beta^2 = 3/4$ is the same with that of $l = 1$, $\alpha^2 = 3/4$ and $\beta^2 = 1/4$ because the two systems have the equal energy [38], which is verified in our numerical simulation. Furthermore, the DBFM with a bosonic VAVSS ($l = 1$) is more stable than the conventional one without vortex ($l = 0$) in the wide range of $N_F < 7943$ because for the bosonic VAVSS there is an additional repulsive centrifugal term $\hbar^2 l^2/(2m_B(x^2 + y^2))$ in the stationary GP equation [38]. When $N_F \geqslant 7943$ all the four different cases of DBFM become instable for N_B above the order of unit. For the DBFMs with a bosonic vortex (VAVSS) of higher l, our simulation shows that the stability curves are similar to the case of $l = 1$, but the systems of higher l are less stable than those of $l = 1$.

IV. CONCLUSION

We have investigated the structure and stability of a quasi-2D DBFM with a bosonic VAVSS, where the BB interaction is taken to be repulsive and the BF interaction to be both repulsive and attractive. It is shown that the bosonic and fermionic density distributions for a DBFM with a bosonic VAVSS in a harmonic plus quartic potential are more tightly confined than those in a harmonic potential. The additional quartic distortion due to experimental uncertainties or artificial quartic confinement does not influence the stationary structure of the mixture, and may favor the sympathetic cooling between the interspecies and makes the system more stable.

Depending on the choice of parameters, the DBFM with a bosonic VAVSS can show rich phase structures. For repulsive BF interaction, the bosonic component can form a petal-shaped "core" inside the honeycomb-like fermionic one, or a ring-shaped joint "shell" around the onion-like fermionic cloud, or multiple segregated "islands" embedded in the disc-shaped Fermi gas. Note that the different separated phases in the DBFM with a bosonic VAVSS are formed under different parameter conditions and can not be achieved by just changing the BF coupling continuously, which is different from the case of a conventional DBFM [14]. In addition, there is a mixing-demixing transition which is controlled by the strength of the BF repulsion. For attractive BF interaction below the threshold for collapse, an almost complete mixing between the bosonic and fermionic components can be formed, where the fermionic component tends to simulate a bosonic VAVSS. Furthermore, we give the stability region for four different cases of DBFM with specific parameters, where the two stability curves of the DBFM with a bosonic VAVSS and the one with a bosonic vortex display an intermittent configuration. These new findings can be verified in the future experiments on DBFMs, and thus the present work provides a new way to test further the validity and prediction of the quantum-hydrodynamic model.

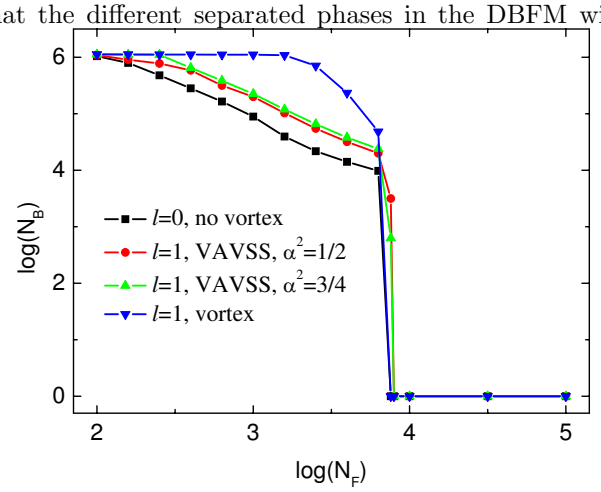

FIG. 5: (color online) Stability region for the degenerate ^{87}Rb-^{40}K mixture with scattering lengths $a_{BB} = 5$ nm and $a_{BF} = -15$ nm. Here the curves of square, circle, triangle, and inverted triangle show the stability limit for the DBFM without vortex, the DBFM with a bosonic VAVSS of $l = 1$ and $\alpha^2 = \beta^2 = 1/2$, the DBFM with a bosonic VAVSS of $l = 1$, $\alpha^2 = 3/4$ and $\beta^2 = 1/4$, and the DBFM with a bosonic vortex of $l = 1$, respectively. For $\log(N_B)$ above the limit or $\log(N_F)$ on the right of the limit the bosonic component or the fermionic one or both the two components collapse simultaneously.

V. ACKNOWLEDGMENTS

The authors sincerely thank Prof. Biao Wu for valuable comments and discussions. This work was supported by the NSFC under Grant No. 10847143, the NSF of Shandong Province under Grant No. Q2007A01, and PhD Foundation of Liaocheng University.

[1] Giorgini S, Pitaevskii L P and Stringari S 2008 *Rev. Mod. Phys.* **80** 1215
[2] Pethick C J and Smith H 2008 *Bose-Einstein condensation in dilute gases* (Cambridge: Cambridge University Press, 2nd edition)
[3] Truscott A G, Strecker K E, McAlexander W I, Partridge G B and Hulet R G 2001 *Science* **291** 2570
[4] Schreck F, Khaykovich L, Corwin K L, Ferrari G, Bourdel T, Cubizolles J and Salomon C 2001 *Phys. Rev. Lett.* **87** 080403
[5] Hadzibabic Z, Stan C A, Dieckmann K, Gupta S, Zwierlein M W, Gorlitz A and Ketterle W 2002 *Phys. Rev. Lett.* **88** 160401
[6] Modugno G, Roati G, Riboli F, Ferlaino F, Brecha R J and Inguscio M 2002 *Science* **297** 2240
[7] Roati G, Riboli F, Modugno G and Inguscio M 2002 *Phys. Rev. Lett.* **89** 150403
[8] Goldwin J, Papp S B, DeMarco B and Jin D S 2002 *Phys. Rev. A* **65** 021402(R)
[9] Ospelkaus C, Ospelkaus S, Sengstock K and Bongs K 2006 *Phys. Rev. Lett.* **96** 020401
[10] Best Th, Will S, Schneider U, Hackermüller L, Oosten D van, Bloch I and Lühmann D -S 2009 *Phys. Rev. Lett.* **102** 030408
[11] Fukuhara T, Sugawa S, Takasu Y and Takahashi Y 2009 *Phys. Rev. A* **79** 021601(R)
[12] Partridge G B, Li W, Kamar R I, Liao Y -a and Hulet R G 2006 *Science* **311** 503
[13] Zwierlein M W, Schunck C H, Schirotzek A and Ketterle W 2006 *Nature* (London) **442** 54
[14] Molmer K 1998 *Phys. Rev. Lett.* **80** 1804
[15] Roth R 2002 *Phys. Rev. A* **66** 013614
[16] Adhikari S K 2004 *Phys. Rev. A* **70** 043617
[17] Akdeniz Z, Minguzzi A, Vignolo P and Tosi M P 2002 *Phys. Rev. A* **66** 013620
[18] Minguzzi A and Tosi M P 2000 *Phys. Lett. A* **268** 142; Akdeniz Z, Vignolo P, Minguzzi A and Tosi M P 2002 *J. Phys. B* **35** L105
[19] Capuzzi P, Minguzzi A and Tosi M P 2003 *Phys. Rev. A* **67** 053605; 2003 *ibid.* **68** 033605; 2004 *ibid.* **69** 053615.
[20] Nygaard N and Molmer K 1999 *Phys. Rev. A* **59** 2974
[21] Viverit L, Pethick C J and Smith H 2000 *Phys. Rev. A* **61** 053605
[22] Roth R and Feldmeier H 2002 *Phys. Rev. A* **65** 021603(R)
[23] Jezek D M, Barranco M, Guilleumas M, Mayol R and Pi M 2004 *Phys. Rev. A* **70** 043630
[24] Adhikari S K 2005 *Phys. Rev. A* **72** 053608
[25] Ma Y L and Chui S T 2002 *Phys. Rev. A* **66** 053611
[26] Hu H and Liu X -J 2003 *Phys. Rev. A* **68** 023608
[27] Santhanam J, Kenkre V M and Konotop V V 2006 *Phys. Rev. A* **73** 013612; Bludov Yu V and Konotop V V 2006 *ibid.* **74** 043616
[28] Salasnich L, Mazzarella G, Salerno M and Toigo F 2010 *Phys. Rev. A* **81** 023614
[29] Fang B, Vignolo P, Miniatura C and Minguzzi A 2009 *Phys. Rev. A* **79** 023623
[30] Maruyama T and Yabu H 2009 *Phys. Rev. A* **80** 043615
[31] Marchetti F M, Jolicoeur Th and Parish M M 2009 *Phys. Rev. Lett.* **103** 105304
[32] Modugno M, Ferlaino F, Riboli F, Roati G, Modugno G and Inguscio M 2003 *Phys. Rev. A* **68** 043626; Liu X -J, Modugno M and Hu H 2003 *Phys. Rev. A* **68** 053605
[33] Chui S T and Ryzhov V N 2004 *Phys. Rev. A* **69** 043607
[34] Takeuchi Y and Mori H 2005 *Phys. Rev. A* **72** 063617
[35] Linder J and Sudbø A 2010 *Phys. Rev. A* **81** 013622
[36] Adhikari S K and Salasnich L 2007 *Phys. Rev. A* **75** 053603
[37] Kapale K T and Dowling J P 2005 *Phys. Rev. Lett.* **95** 173601
[38] Liu M, Wen L H, Xiong H W and Zhan M S 2006 *Phys. Rev. A* **73** 063620
[39] Simula T P, Nygaard N, Hu S X, Collins L A, Schneider B I and Molmer K 2008 *Phys. Rev. A* **77** 015401
[40] Thanvanthri S, Kapale K T and Dowling J P 2008 *Phys. Rev. A* **77** 053825
[41] Wen L H, Wang J S, Feng J and Hu H Q 2008 *J. Phys. B* **41** 135301
[42] Andersen M F, Ryu C, Cladé P, Natarajan V, Vaziri A, Helmerson K and Phillips W D 2006 *Phys. Rev. Lett.* **97** 170406
[43] Wright K C, Leslie L S and Bigelow N P 2008 *Phys. Rev. A* **77** 041601(R); Wright K C, Leslie L S, Hansen A and Bigelow N P 2009 *Phys. Rev. Lett.* **102** 030405
[44] Adhikari S K 2005 *J. Phys. B* **38** 3607; 2006 *Laser Phys. Lett.* **3** 605
[45] Salasnich L, Adhikari S K and Toigo F 2007 *Phys. Rev. A* **75** 023616
[46] Karpiuk T, Brewczyk K, Ospelkaus-Schwarzer S, Bongs K, Gajda M and Rzazewski K 2004 *Phys. Rev. Lett.* **93** 100401
[47] Andreev P A and Kuzmenkov L S 2008 *Phys. Rev. A* **78** 053624
[48] Subaşi A L, Sevinçli S, Vignolo P and Tanatar B 2009 *Phys. Rev. A* **79** 063632
[49] Fetter A L, Jackson B and Stringari S 2005 *Phys. Rev. A* **71** 013605
[50] Li G Q, Fu L B, Xue J K, Chen X Z and Liu J 2006 *Phys. Rev. A* **74** 055601
[51] Zhang Y P and Wu B 2009 *Phys. Rev. Lett.* **102** 093905
[52] Wen L H, Xiong H W and Wu B *arXiv*:1003.2798
[53] Wen L H and Li J H 2007 *Phys. Lett. A* **369** 307
[54] Ferrari G, Inguscio M, Jastrzebski W, Modugno G, Roati G and Simoni A 2002 *Phys. Rev. Lett.* **89** 053202